A mouse model of *MYCN*-driven retinoblastoma reveals *MYCN*-independent tumor reemergence

Nan Wu,[1] Deshui Jia,[1] Breanna Bates,[1] Ryan Basom,[2] Charles G. Eberhart,[3] and David MacPherson[1,4]

[1]Divisions of Human Biology and Public Health Sciences and [2]Genomics and Bioinformatics Shared Resource, Fred Hutchinson Cancer Research Center, Seattle, Washington, USA. [3]Divisions of Pathology, Ophthalmology, and Oncology, Johns Hopkins University School of Medicine, Baltimore, Maryland, USA. [4]Department of Genome Sciences, University of Washington, Seattle, Washington, USA.

The most frequent focal alterations in human retinoblastoma are mutations in the tumor-suppressor gene retinoblastoma (*RB*) and amplification of the oncogene *MYCN*. Whether *MYCN* overexpression drives retinoblastoma has not been assessed in model systems. Here, we have shown that *Rb* inactivation collaborates strongly with *MYCN* overexpression and leads to retinoblastoma in mice. Overexpression of human *MYCN* in the context of *Rb* inactivation increased the expression of MYC-, E2F-, and ribosome-related gene sets, promoted excessive proliferation, and led to retinoblastoma with anaplastic changes. We then modeled responses to MYCN-directed therapy by suppressing *MYCN* expression in *MYCN*-driven retinoblastomas. Initially, *MYCN* suppression led to proliferation arrest and partial tumor regression with loss of anaplasia. However, over time, retinoblastomas reemerged, typically without reactivation of human *MYCN* or amplification of murine *Mycn*. A subset of returning retinoblastomas showed genomic amplification of a *Mycn* target gene encoding the miR cluster miR-17~92, while most retinoblastomas reemerged without clear genetic alterations in either *Mycn* or known *Mycn* targets. This *Rb/MYCN* model recapitulates key genetic driver alterations seen in human retinoblastoma and reveals the emergence of *MYCN* independence in an initially *MYCN*-driven tumor.

Introduction

MYC family members (*MYC, MYCN, MYCL*) are among the most frequently amplified oncogenes in human cancers. *MYCN* amplifications have long been known to contribute to human retinoblastoma, often together with retinoblastoma (*RB*) loss (1, 2). *MYCN* is also amplified in a small subset of human retinoblastomas harboring an intact *RB* gene (3). Despite frequent amplifications of *MYCN* in human retinoblastomas, the mechanisms underlying *MYCN* oncogenic activity in retinoblastoma have been largely unexplored. *MYCN* and *RB* also cooperate in tumorigenesis beyond retinoblastoma. For example, *MYCN* is frequently amplified in neuroblastoma, and *Rb* deletion in mice accelerated *MYCN*-driven neuroblastoma (4). Also, in human small-cell lung cancer, *RB* deletions and *MYCN* amplifications co-occur (5). A better understanding of how *RB* loss cooperates with *MYCN* overexpression in tumorigenesis is needed.

MYCN is a basic helix-loop-helix transcription factor that dimerizes with MYC-associated factor X (MAX) and can activate transcription via binding to E-box elements and noncanonical sites. MYCN and MYC can activate target genes such as *Mir-17-92*, which encodes the oncogenic miR cluster miR-17~92 (6–8). MYC family members regulate RNA Pol I, II, and III activities and broadly increase mRNA translation (9). MYC family members also globally increase the transcriptional output of actively transcribed genes (10, 11), in part by recruiting the pause-release factor pTEFb to promote transcriptional elongation (12). Inactivation of *Mycn* in mice led to nuclear condensation, reduced histone acetylation, and global changes in histone methylation (13). MYCN regulates proliferation, differentiation, and global chromatin organization; with these pleiotropic activities, the key oncogenic functions of *MYCN* remain unclear.

Recent strategies have emerged to therapeutically target MYCN-dependent tumors by reducing MYCN expression. MYCN stability is regulated by aurora kinase A, whereby binding to aurora kinase A can protect MYCN protein from degradation (14). Aurora kinase A inhibitors destabilized MYCN, suggesting a therapeutic strategy for combating *MYCN*-amplified tumors (15, 16). Other promising approaches for targeting *MYCN*-amplified tumors include inhibition of BET domain proteins (17) or of CDK7 (18), both of which lead to reduced *MYCN* transcription. Despite excitement about the potential of targeted therapies to decrease *MYCN* expression in *MYCN*-amplified tumors, whether resistance to *MYCN*-directed therapies will occur has not been determined in any model system.

Mouse models provide ideal tools to understand the mechanisms underlying oncogene function and to model the development of therapy resistance. Inducible models can be used to test the continued requirement for an initiating oncogenic alteration. Unlike in humans, germline *Rb* heterozygosity in mice does not lead to retinoblastoma (19–21). Inactivation of both copies of *Rb* in the earliest stages of retinal development led to extension of the proliferative period of retinal development, but eventually, cells exited the cell cycle or underwent apoptosis (22, 23). For mice to develop retinoblastoma in past models, *Rb* needed to be inactivated together with another *Rb* family member, *Rb1* (also known as *p107*) (22, 24–26) or *Rbl2* (also known as *p130*) (23, 27), or the CDK inhibitor *Cdkn1b* (also known as *p27*) (28). *MYCN* is the most frequently focally altered gene in human retinoblasto-

Conflict of interest: The authors have declared that no conflict of interest exists.
Submitted: May 10, 2016; **Accepted:** December 15, 2016.
Reference information: *J Clin Invest*. 2017;127(3):888–898.
https://doi.org/10.1172/JCI88508.

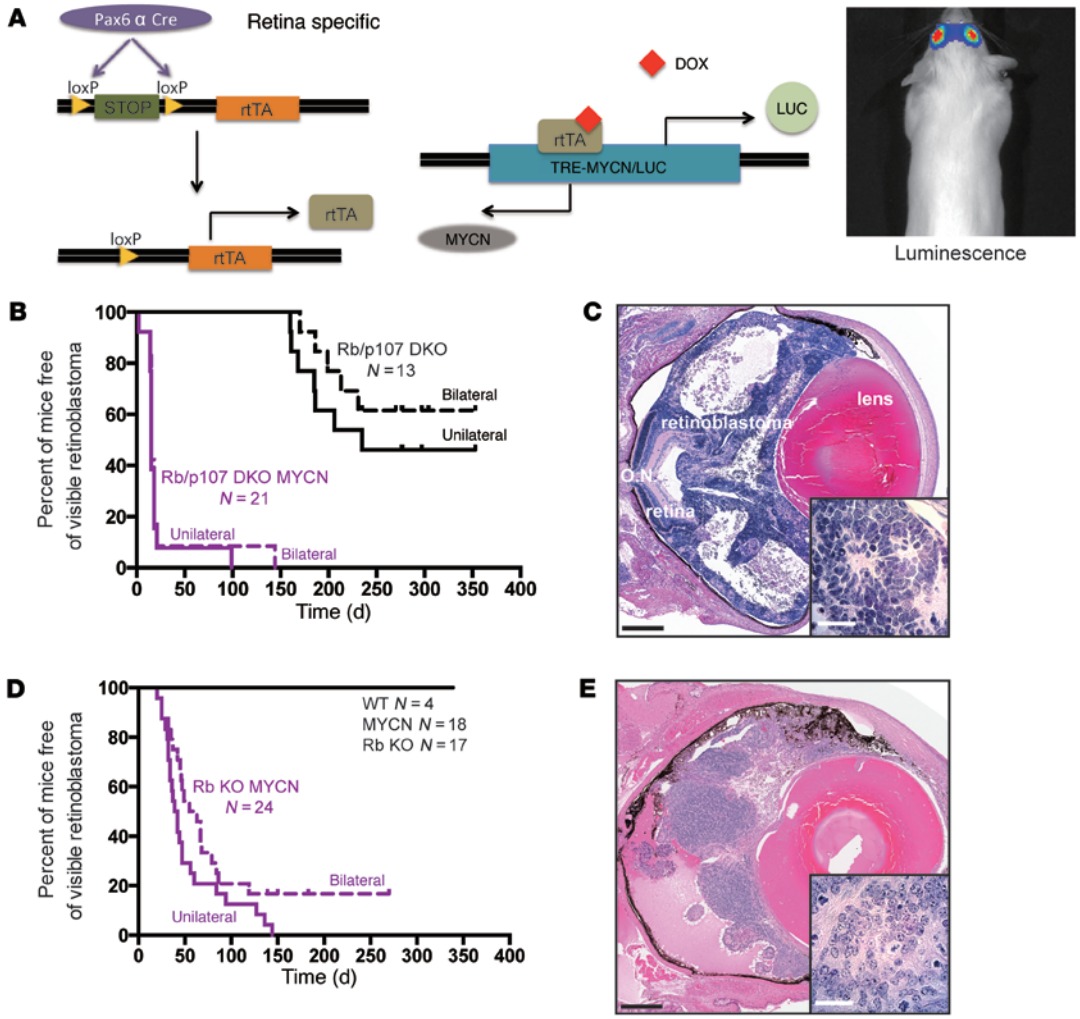

Figure 1. *MYCN* overexpression cooperates with *Rb* loss to drive retinoblastoma. (**A**) Strategy to overexpress *MYCN* in *Rb* or *Rb/p107*-deficient retina. Retina-specific *Pax6* α enhancer *Cre* (Pax6 α Cre) drives the expression of rtTA in the developing retina. The *TRE-MYCN* allele allowed for DOX-dependent expression of MYCN and luciferase in the retina. Image shows an in vivo assessment of bioluminescence in a tumor-bearing animal. (**B**) Kaplan-Meier curve shows the time to externally evident retinoblastoma in *Rb/p107* (Rb/p107 DKO) compared with *Rb/p107/TET-MYCN* (Rb/p107 DKO MYCN) mice. The time to tumor presence in the first eye (unilateral curve) and second eye (bilateral curve) is shown. (**C**) H&E-stained eye from an *Rb/p107/TET-MYCN* mouse at P12, showing extensive retinoblastoma. The inset image is of tumor cells (original magnification, ×100) and shows Homer Wright rosettes typical of human and mouse retinoblastomas. O.N., optic nerve. (**D**) Kaplan-Meier curve showing the time to unilateral and then bilateral retinoblastoma formation in *Rb/TET-MYCN* (Rb KO MYCN) mice. (**E**) H&E staining of retinoblastoma-containing eye from an *Rb/TET-MYCN* model (inset: original magnification, ×100). Black scale bar: 500 μm; white scale bar: 25 μm.

ma beyond *RB* (2), and so we sought to control *MYCN* expression in the mouse retina harboring *Rb* family member deletion. We report a model of retinoblastoma that precisely mimics key genetic alterations in human retinoblastoma tumors and obviates any need to genetically inactivate *Rb* family members beyond *Rb*. This model was an ideal system for determining whether *MYCN* is required for retinoblastoma maintenance and for identifying features of tumors that become *MYCN* independent.

Results

To explore roles for *MYCN* in retinoblastoma, we used a TET-ON–inducible system, in which human *MYCN* can be controllably overexpressed (29) (Figure 1A). Here, a retina-specific Cre driver (*Pax6* α enhancer *Cre*) (30) is coupled with a lox-stop-lox reverse tetracycline transactivator (rtTA) allele to lead to rtTA expression specifically in early retinal progenitor cells (beginning near E10) and their daughter cells. In the presence of a tetracycline-responsive element–MYCN/firefly luciferase (*TRE-MYCN/LUC*) allele (29) containing a tetracycline response element, human *MYCN*, and a luciferase reporter, doxycycline (DOX) addition to the food leads to overexpression of both *MYCN* and luciferase that can be monitored in vivo. Mice with the combination of LoxP-Stop-LoxP–reverse Tet transactivator (*LSL-rtTA*) *TRE-MYCN/LUC Pax6* α enhancer *Cre* alleles are referred to herein as *TET-MYCN* mice.

MYCN overexpression accelerates Rb/p107-deleted retinoblastoma. We examined whether *TET-MYCN* would synergize with *Rb* family member loss to promote retinoblastoma. In a previous mouse model harboring conditional *Rb* and *p107* deletion in the retina (genotype *Pax6* α enhancer *Cre* $Rb^{fl/fl}$ $p107^{fl/fl}$, referred to hereafter as *Rb/p107* mice), retinoblastomas arose with long latency. *MYCN* was

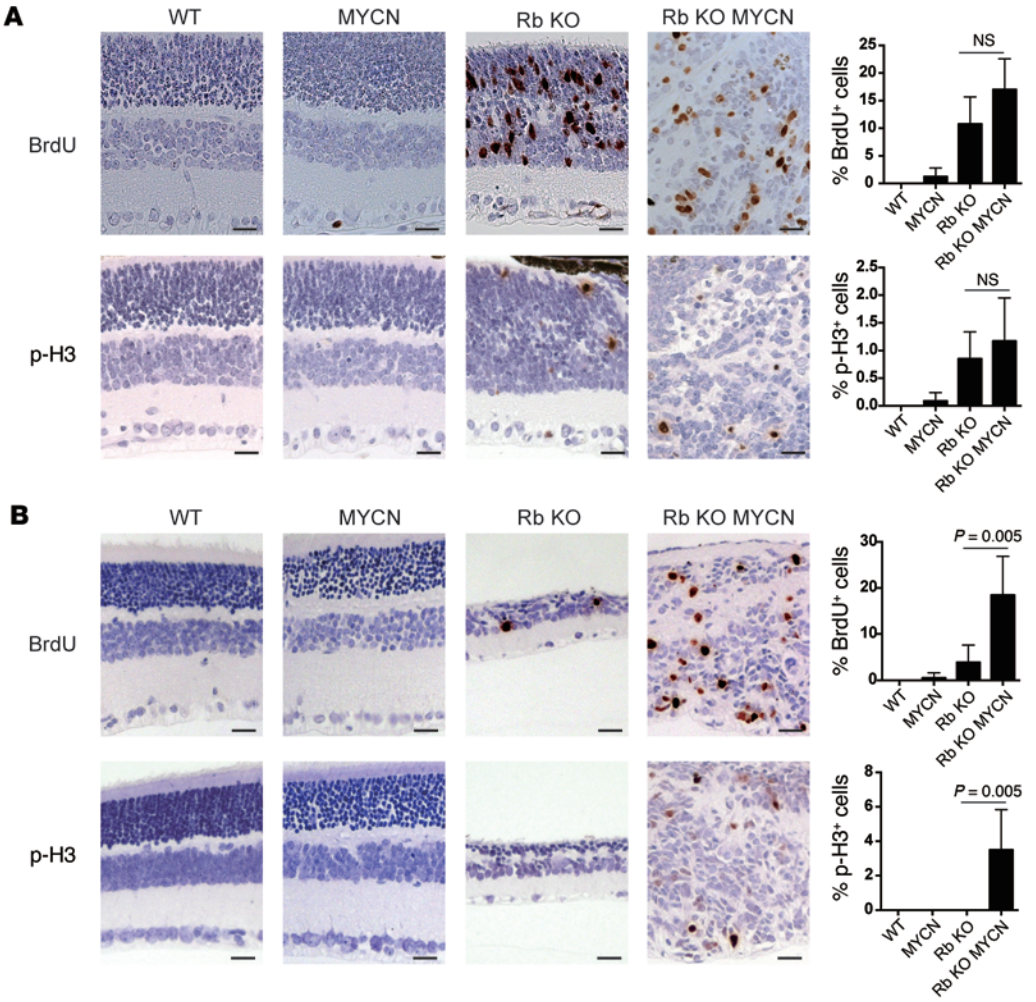

Figure 2. *MYCN* cooperates with *Rb* inactivation to increase proliferation in the retina. (**A**) Brdu and p-H3 analysis of retinae at P12 showing increased proliferation in *Rb*-null (Rb KO) and *Rb/TET-MYCN* (Rb KO MYCN) retinae relative to control or *MYCN*-only retinae. *N* = 4–7 independent retinae, with 1 section examined per retina. (**B**) BRDU and p-H3 analysis at P22 shows increased proliferation in *Rb/TET-MYCN* retinae relative to *Rb*-deficient retinae that had largely exited the cell cycle. *N* = 4–6 independent retinae, with 1 section per retina. Scale bar: 25 μm. Error bars represent the SD. *P* values shown in **B** were determined by 2-tailed Student's *t* test.

spontaneously amplified in a subset of mice from this model (24), just as *MYCN* is amplified in human retinoblastomas. We used the *Rb/p107* model to now overexpress *MYCN* (referred to hereafter as *Rb/p107/TET-MYCN* mice). To induce *MYCN* during retinal development, we fed DOX-containing chow to breeders throughout their pregnancy and before weaning, such that *MYCN* was overexpressed throughout retinal development and into adulthood. *Rb/p107/TET-MYCN* animals were followed until they developed advanced retinoblastoma. We found that overexpression of *MYCN* dramatically accelerated the time to retinoblastoma (Figure 1B). *Rb/p107* mice developed retinoblastoma with only partial penetrance, and starting at about 5 months of age, *Rb/p107/TET-MYCN* mice exhibited bilateral retinoblastomas, typically from the time that their eyes opened (Figure 1, B and C). Thus, *MYCN* potently synergizes with *Rb/p107* loss to promote retinoblastoma.

MYCN overexpression with Rb deletion alone drives retinoblastoma. We next examined the effects of *MYCN* overexpression on retinae lacking *Rb* but with *p107* intact (*Rb/TET-MYCN* mice). Remarkably, *MYCN* overexpression promoted retinoblastoma in the *Rb*-mutant context, bypassing any need to inactivate *p107* or *p130* (Figure 1, D and E). *Rb/TET-MYCN* mice developed retinoblastoma with very rapid kinetics (average of 54 days) and complete penetrance. While a subset of retinoblastoma patients who harbor *MYCN* amplification but not *RB* mutation has been described (3), we found no effect of *MYCN* overexpression on retinoblastoma when *Rb* was WT (Figure 1D). *MYCN* overexpression cooperated with *Rb* loss to lead to rapid retinoblastoma when DOX was present during retinal development (Figure 1, D and E). Interesting morphological changes were also noted when comparing retinoblastomas in the *Rb/TET-MYCN* mouse model with those in the *Rb/p107* and *Rb/p107/TET-MYCN* mouse models. Tumors arising in *Rb/p107* mice were composed of small, round blue cells with scattered apoptotic bodies and mitotic figures (Supplemental Figure 1A; supplemental material available online with this article; https://doi.org/10.1172/JCI88508DS1). In some animals, neuroblastic Homer Wright rosettes were present. In *Rb/TET-MYCN* mice, tumor cells were somewhat larger and more often elongated, angular, or molded together (Supplemental Figure 1B) — anaplastic features that have been associated with *MYCN* amplification in human retinoblastoma and worse clinical outcomes (3, 31). We found that anaplastic changes were even more prominent in *Rb/p107/TET-MYCN* tumors (Supplemental Figure 1C).

We hypothesized that retinoblastoma, a pediatric cancer, would require MYCN overexpression to occur during retinal development to lead to retinoblastoma. Indeed, when we administered DOX to adult 3-week-old mice, retinoblastoma emerged in only 1 of 20 *Rb/TET-MYCN* mice (Supplemental Figure 2). This result indicates that there is a critical window during retinal

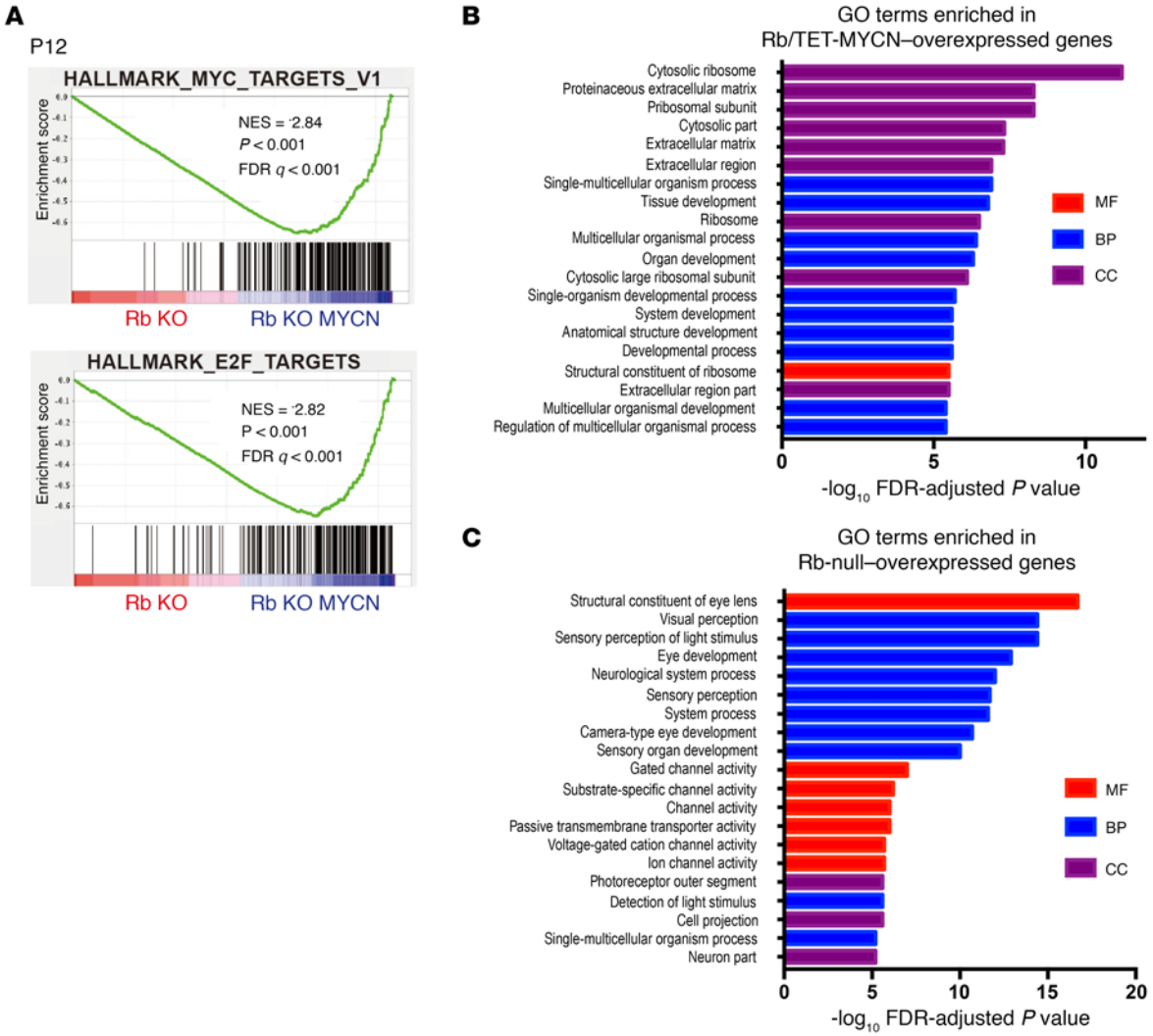

Figure 3. Gene expression changes with *MYCN* overexpression in *Rb*-deleted retina. (**A**) GSEA comparing *Rb*-null ($n = 4$) with *Rb/MYCN* ($n = 4$) retinae at P12. The 50-gene "Hallmark signatures" set from MSigDB was queried and showed MYC- and E2F-related gene sets as the top 2 most significant gene sets enriched upon *MYCN* overexpression in the *Rb*-null retina. (**B**) Top 10 gene sets enriched in *Rb/TET-MYCN* and top 3 gene sets in *Rb*-null P12 retinae, with the normalized enrichment score (NES) shown. (**C**) Enriched GO terms in genes upregulated in *Rb/TET-MYCN* relative to *Rb*-null P12 retinae. (**D**) Enriched GO terms in genes upregulated in *Rb*-null relative to *Rb/TET-MYCN* P12 retinae. MF, molecular function; BP, biological process; CC, cellular component.

development, prior to P21, for *MYCN* overexpression to efficiently cooperate with *Rb* loss in promoting retinoblastoma.

MYCN overexpression synergizes with Rb loss to bypass a proliferative block. To examine mechanisms underlying the observed synergy between *MYCN* and *Rb* loss, we analyzed mutant retinae at 2 time points, P12 and P22. We examined proliferation using BrdU and anti-Ser10 phosphorylated histone H3 (p-H3) immunohistochemical analysis and apoptosis using a TUNEL assay. At P12, when cells in control retinae had stopped proliferating, *Rb* and *Rb/TET-MYCN* retinae exhibited extensive proliferation and apoptosis (Figure 2A and Supplemental Figure 3). We found no significant differences in proliferation or apoptosis levels between these genotypes. By P22, however, proliferation in the *Rb*-mutant retina had nearly ceased, and retinae in the *Rb* KO model were hypocellular owing to prior apoptosis. In contrast, proliferation continued unabated in the *Rb/TET-MYCN* retinae (Figure 2B). Thus, *MYCN* overexpression bypasses a proliferation block that otherwise occurs in the *Rb*-deficient retina. To identify gene expression changes driven by *MYCN* in the *Rb*-deficient retina, we focused on the earlier P12 stage, when there was no significant difference in overall proliferation levels between *Rb* and *Rb/TET-MYCN*–mutant retinae. Gene set enrichment analysis (GSEA) using RNA-sequencing (RNA-seq) data revealed both MYC-associated and E2F-associated gene sets as the top 2 most highly enriched gene sets in the *Rb/MYCN* condition compared with *Rb* alone (Figure 3A and Supplemental Table 1). Enrichment of E2F-associated gene sets compared with *Rb*-mutant retinae suggests that gene expression programs promoted by *Rb* loss may be strengthened by *MYCN* overexpression. We also used the edgeR package (32) to identify significant differentially expressed genes (Supplemental Table 2). Analyses of enriched Gene Ontology (GO) terms also revealed ribosome-, extracellular matrix–, and tissue development–associated genes to be enriched in the *Rb/MYCN*-overexpressed transcripts when

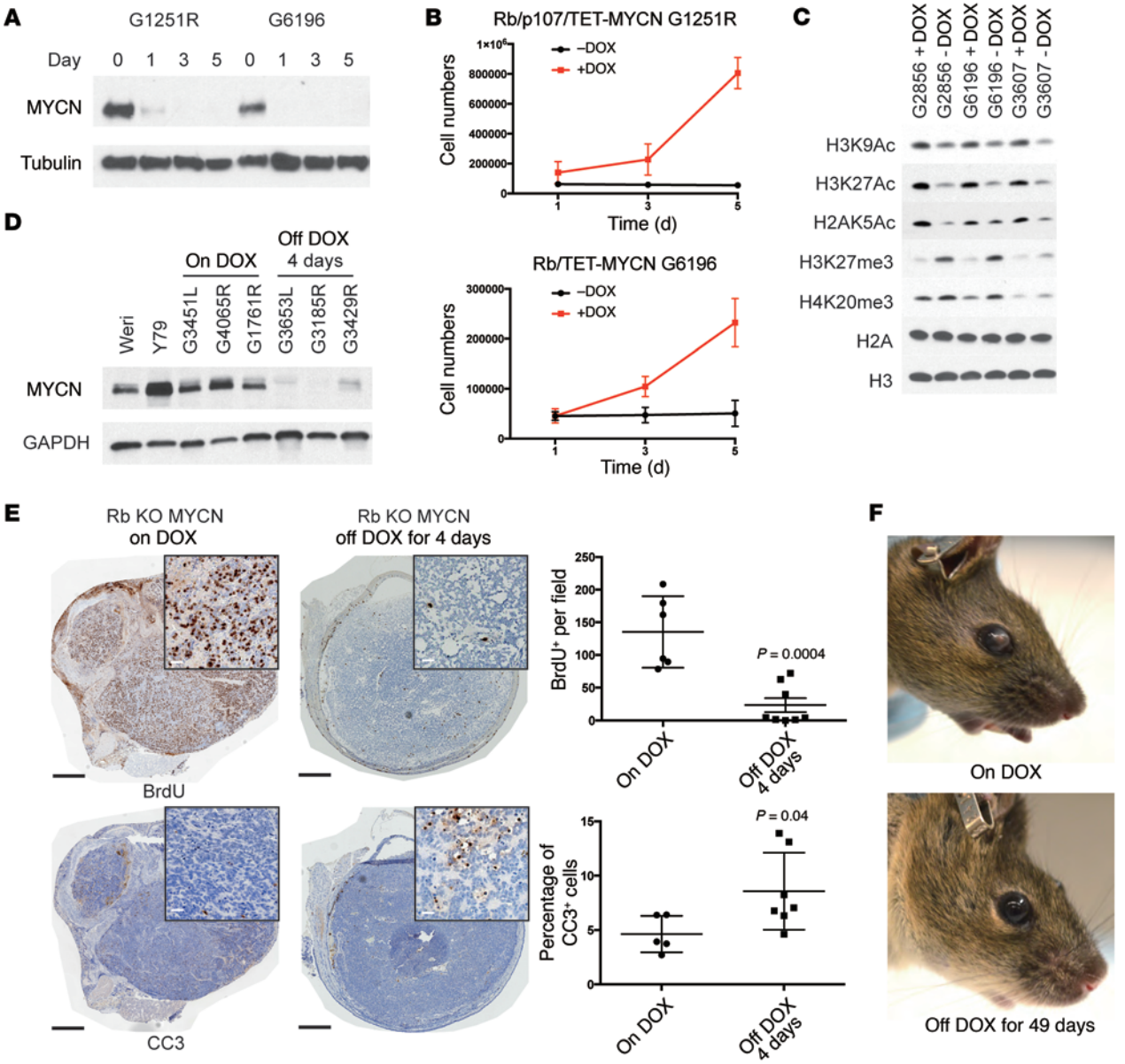

Figure 4. Sustained MYCN expression is initially required for retinoblastoma cell proliferation. DOX removal in cell lines derived from *Rb/TET-MYCN* tumors led to (**A**) reduced MYCN protein expression on Western blotting and (**B**) proliferation impairment, as assessed by counting cells 1, 3, and 5 days after plating. Data were pooled from 3 independent experiments. (**C**) Western blot of histone extracts from 3 *Rb/TET-MYCN* cell lines showing reduced histone H3K9, H3K27, and H2A K5 acetylation (Ac) and increased H3K27 and H4K20 trimethylation (me3) upon removal of DOX from the media. Individual blots indicating equal loading are shown Supplemental Figure 4D. (**D**) DOX removal in vivo initially resulted in suppression of MYCN protein expression by day 4. (**E**) Immunohistochemical analysis shows decreased BrdU-positive cells and increased cleaved caspase 3 (CC3) levels 4 days after DOX removal. Black scale bars: 500 μm; white scale bars (insets): 25 μm. Plot shows quantification from 5 to 8 independent retinae per genotype. The *P* values were determined by Student's *t* test. (**F**) Photographs showing a mouse with retinoblastoma in the anterior chamber, compared with 49 days later when the tumor had regressed.

compared with *Rb*-null retinae (Figure 3B). The most significant GO term was "cytosolic ribosome" (FDR-adjusted *P* value = 6.6×10^{-12}), consistent with MYCN activation of ribosomal biogenesis–associated gene expression programs (33). Genes overexpressed in the *Rb*-null relative to *Rb/TET-MYCN* retinae at P12 included genes involved in eye/retina development (Figure 3C). The phenotypic data, along with gene expression changes, including enrichment of E2F target gene sets with *MYCN* overexpression, support the notion that *MYCN* drives proliferation programs in *Rb*-null cells to promote retinoblastoma. This is consistent with our finding that *MYCN* overexpression obviates the need for inactivation of other negative cell-cycle regulators to induce retinoblastoma (such as the other Rb family members *p107*, *p130*, and *p27*).

Suppression of MYCN expression in retinoblastoma cells. To determine whether maintenance of *MYCN* expression is important for retinoblastoma cells in culture, we generated cell lines from *Rb/TET-MYCN* and *Rb/p107/TET-MYCN* retinoblastomas in the presence of DOX. Removal of DOX led to a rapid loss of MYCN protein (Figure 4A) and suppression of proliferation (Fig-

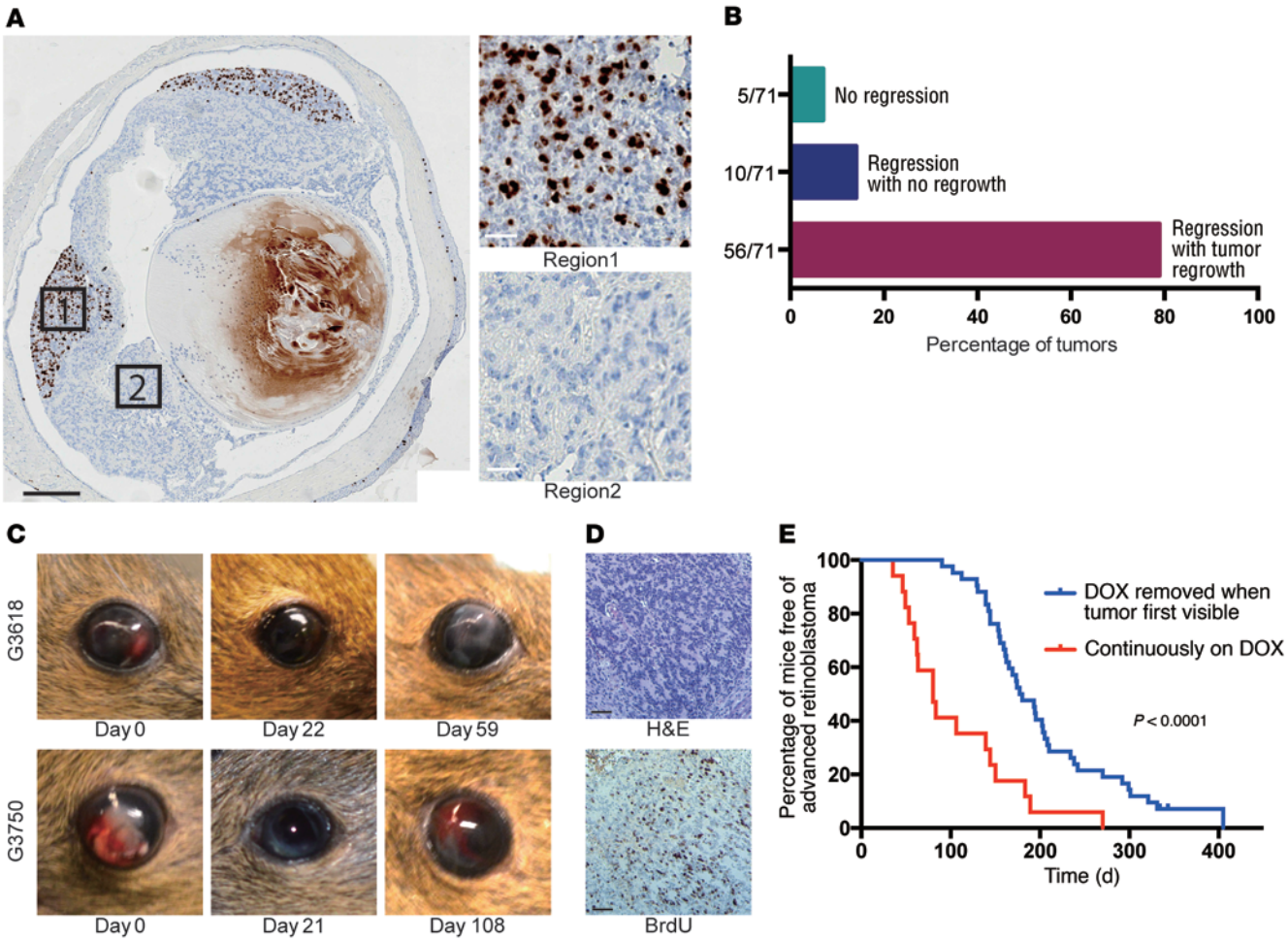

Figure 5. *MYCN*-independent retinoblastomas emerge in the absence of DOX. (**A**) BrdU analysis showing regions with extensive proliferation in *Rb/TET-MYCN* retinae in the DOX-OFF condition 27 days after DOX removal, while other regions were nonproliferative. Black scale bar: 500 μm; white scale bars: 25 μm. Five of twelve eyes examined showed pockets of proliferation, with one section examined per eye. (**B**) Histogram showing the proportion of eyes with no tumor regression upon DOX removal, with regression but no regrowth, and with regression followed by DOX-independent tumor regrowth. (**C**) Photographs showing tumor regression upon DOX removal and then reappearance in the anterior chamber of the eye in 2 animals. (**D**) BrdU analysis showing a high proliferation rate in DOX-independent returned tumor. Scale bars: 50 μm. (**E**) Kaplan-Meier curves showing the time to development of late-stage retinoblastoma filling the eye. *Rb/TET-MYCN* mice were either maintained continuously on DOX (n = 17), or had DOX removed from their diet when the retinoblastoma was first externally visible in the eye (n = 42), usually with tumor evident in the anterior chamber. The P value shown was determined by log-rank test.

ure 4B) that was associated with G_1 block (Supplemental Figure 4A). The cells exhibited an enlarged and flattened morphology (Supplemental Figure 4B) and stained positively for senescence-associated β-gal (SA-β-gal) (Supplemental Figure 4C). *MYCN* has been found to control global chromatin structure, with *MYCN*-deficient neural progenitor cells exhibiting global hypoacetylation (13). To examine the effects of *MYCN* suppression on global histone marks, we performed Western blotting of extracted histones. Removal of DOX led to global reduction in acetylation at a number of sites associated with active chromatin, including H3K9, H3K27, and H2AK5, and led to increases in repressive marks such as H3K27 and H4K20 trimethylation (Figure 4C and Supplemental Figure 4D). Acute *MYCN* suppression in retinoblastoma cells led to the suppression of proliferation and changes in histone modifications that are generally associated with repressive chromatin.

Suppression of MYCN expression in MYCN-driven tumors leads to cell-cycle arrest and partial tumor regression. Several studies have reported on potential MYCN-directed therapeutic approaches to reduce MYCN expression levels (14–18). One approach involves inhibition of aurora kinase A, which is required for MYCN protein stability (14–16). We found that *MYCN* overexpression in retinoblastoma cell lines conferred sensitivity to aurora kinase A inhibition using MLN8237 (alisertib) (Supplemental Figure 5, A–C). MLN8237 treatment led to reduced MYCN protein levels and activation of p53 in an *Rb/TET-MYCN* retinoblastoma cell line (Supplemental Figure 5B). Two *Rb/TET-MYCN* and two *Rb/p107/TET-MYCN* cell lines were highly sensitive to MLN8237 in the DOX-ON condition (Supplemental Figure 5C). Removal of DOX from the media of these cell lines suppressed MYCN expression and strongly reduced the effectiveness of MLN8237, suggesting that the effectiveness of aurora kinase A inhibition was MYCN dependent. DOX removal led to decreased proliferation upon MYCN suppression, which could have affected the MLN8237 response; thus, we also compared MLN8237 activity in retinoblastoma cells that differed in MYCN expression levels but that had similar proliferation rates. In cell lines derived from

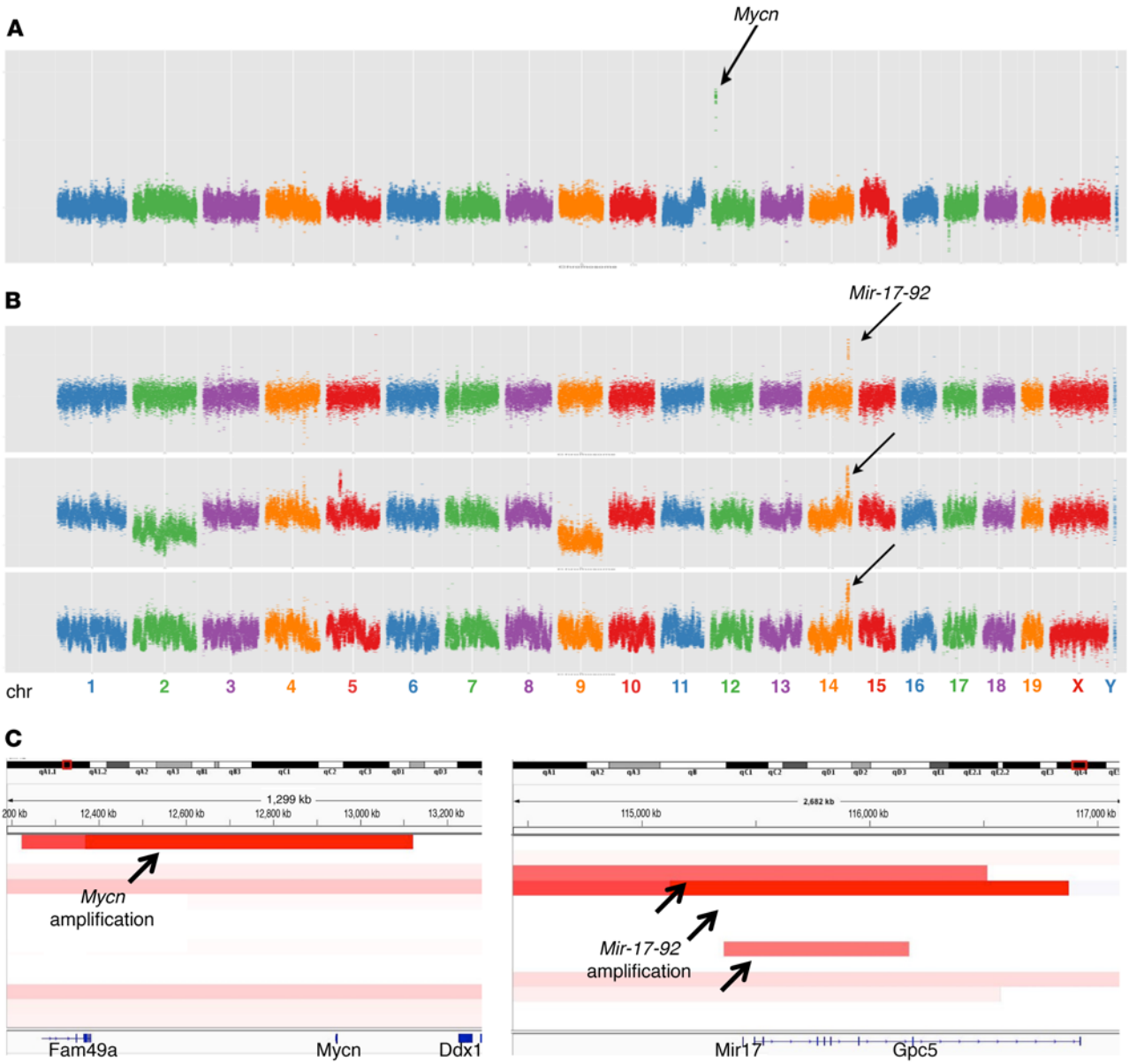

Figure 6. Focal amplifications in *Rb/TET-MYCN* DOX-independent tumors. CNV profiles of samples harboring focal amplifications in (**A**) *Mycn* or (**B**) *Mir-17-92*. Low-coverage whole-genome sequencing data were analyzed using CNVSeq. Arrows point to focal amplifications. chr, chromosome. (**C**) Integrative Genomics Viewer (IGV) (http://software.broadinstitute.org/software/igv/) plot showing the genomic regions of *Mycn* and *Mir-17-92* amplification.

Rb/p107 retinoblastomas, in which MYCN protein levels were very low, there was a strikingly reduced effect of MLN8237 compared with cell lines from *Rb/p107/TET*-MYCN retinoblastomas (Supplemental Figure 5, D and E). Thus, the inhibitory effect of MLN8237 was specific to *MYCN*-overexpressing retinoblastoma cells. These data indicate that *MYCN*-directed therapy acts in a *MYCN*-specific manner in retinoblastoma cells.

We hypothesized that retinoblastomas initiated by *Rb* inactivation and *MYCN* overexpression would maintain a continued requirement for *MYCN* expression, given the complete absence of retinoblastoma in mice lacking Rb alone (22, 23, 34). To test this hypothesis, we removed DOX from the feed of retinoblastoma-bearing *Rb/TET-MYCN* animals. Four days after DOX removal, MYCN protein levels were suppressed (Figure 4D), and we found a strong decrease in BrdU-positive cells along with an increase in apoptosis, as shown by cleaved caspase 3 immunohistochemical analysis (Figure 4E). Histological changes were also evident 4 days after DOX removal, as the reduction in MYCN expression was associated with a round, regular tumor cell morphology, suggesting increased differentiation as well as a dramatic reduction in mitotic figures (Supplemental Figure 1D). In contrast to the phenotype observed in cell culture, where DOX removal led to features of senescence, we found no evidence of senescence in vivo 4 days or 27 days after DOX removal. Tumors did not stain for SA-β-gal 4 or 27 days after DOX removal (Supplemental Figure 6A), and we did not observe an upregulation of a panel of senescence-associated transcripts such as *p21* or *p16* or senescence-associated cytokines (Supplemental Figure 6B). In 66

of 71 tumor-bearing eyes, complete elimination of retinoblastoma in the anterior chamber of the eye was eventually observed with DOX removal (average time of 21 ± 13 days) (Figure 4F and Figure 5B). The early response to MYCN suppression was suppression of tumor proliferation, increased cell death, and tumor elimination from the anterior chamber of the eye.

MYCN-independent proliferation and tumor reemergence. We next determined whether the proliferation arrest associated with MYCN suppression in vivo would be sustained over time. Twenty-seven days after DOX removal, we performed BRDU analysis. In 5 of 12 eyes, we found pockets of extensive proliferation, while other regions of the retinoblastoma were nonproliferative (Figure 5A). We followed mice for a return of tumor to the anterior chamber of the eye. In 56 of the 66 eyes that showed tumor regression from the anterior chamber, we found that tumors eventually returned (Figure 5, B and C). The average time to relapse was 87 ± 51 days, and when tumors returned, they were highly proliferative (Figure 5D). We followed mice beyond the time of the tumor's first appearance in the eye to when morbidity from advanced retinoblastoma filling the eye occurred and euthanasia was required. We compared cohorts with or without DOX removal at the first appearance of tumor cells in the eye and found that the mice with DOX removal had significantly increased survival, free of advanced retinoblastoma filling the eye (Figure 5E). One mechanism associated with DOX-independent growth of tumors driven by a DOX-inducible oncogene could be reactivation of the initiating oncogene. For example, *rtTA* mutations could occur that render the allele DOX independent (35). Examination of 27 tumors that had returned using quantitative real-time PCR to assess transgenic human *MYCN* expression showed that only 1 tumor had high *MYCN* expression levels (Supplemental Figure 7A). This tumor also had high levels of luciferase bioluminescence (not shown), suggesting a rare occurrence of DOX-independent activation of *rtTA* in this sample. We did not observe widespread upregulation of endogenous murine *Mycn, Myc*, or *Mycl* in the DOX-independent tumors (Supplemental Figure 7B). Thus, reactivating the initiating oncogene *MYCN* was not a frequent cause of DOX-independent retinoblastoma regrowth in this model. Previous mouse models relied on mutation of other *Rb* family members or p27, together with *Rb* inactivation, to induce retinoblastoma. We found no loss of p107, p130, or p27 in a group of tumors that returned in the absence of DOX (Supplemental Figure 8).

Amplification of Mir-17-92 in a subset of DOX-independent tumors. To identify genetic changes that occur in *MYCN*-independent retinoblastomas, we performed copy number variation (CNV) analyses, comparing DNA copy numbers in the tumor relative to normal tail DNA. We used low-coverage whole-genome sequencing to identify regions of deletion and amplification in *Rb/TET-MYCN* (DOX-ON) versus *Rb/TET-MYCN* (DOX-OFF) retinoblastomas and found whole chromosome gains and losses in the *MYCN*-ON condition but did not see focal amplifications. In contrast, we now observed focal amplifications in the *MYCN*-OFF condition. One of thirteen DOX-independent samples showed *Mycn* genomic amplification (Figure 6, A and C). More frequently, recurrent focal amplifications were found not in *Mycn* but rather in a key *MYCN* target gene, *Mir-17-92*, which encodes the miR-17~92 cluster (Figure 6, B and C). To expand upon this result, we performed quantitative real-time PCR for *Mir-17-92* copy numbers across a larger sample set and found that 4 of 26 tumors harbored *Mir-17-92* amplifications in the MYCN-OFF group, while 0 of 25 harbored *Mir-17-92* amplifications in the MYCN-ON group (Supplemental Figure 9A). We did not expect to see *Mir-17-92* amplifications in the *MYCN*-ON group, as *Mir-17-92* is a well-characterized direct MYCN target gene (7, 36–38). We next determined whether enforced expression of *Mir-17-92* would allow *Rb/TET-MYCN* cells to continue to cycle upon DOX removal and the consequent MYCN suppression. We used a murine stem cell virus–Mir-17-92 (MSCV–*Mir-17-92*) retroviral vector (39) to overexpress *Mir-17-92* in 2 *Rb/TET-MYCN* cell lines. We achieved expression of miR-17 at levels similar to those found in the *Rb/TET-MYCN* DOX-ON condition (Supplemental Figure 9B). However, *Mir-17-92* overexpression did not rescue the proliferation arrest caused by DOX removal and *MYCN* suppression in either cell line (Supplemental Figure 9C). Thus, a subset of retinoblastomas that had evolved DOX independence exhibited amplification of a key MYCN target gene, while the majority of these tumors did not show focal amplifications or deletions of *MYCN* or its targets.

Discussion

We show that *MYCN* acts as a potent oncogene in *Rb*-deficient retinoblastoma. *RB* deletion and *MYCN* amplification are the two most frequent focal alterations occurring in human retinoblastoma, and these alterations often co-occur in the same tumor (2). *MYCN* amplifications in the absence of *RB* mutations or deletions have been described previously (2, 3). In one study, high-level *MYCN* amplifications were found only in those retinoblastomas in which *RB* mutations were undetected (3). In a more recent study, however, 8 of 94 retinoblastomas had more than 10 *MYCN* copies, and 6 of 8 of these *MYCN*-amplified retinoblastomas had at least 1 hit in the *RB* gene detected (2). Thus, a subset of retinoblastomas shows *MYCN* amplification, even in the absence of detected *RB* mutation, while in other retinoblastomas, *MYCN* amplification and *RB* mutations co-occur. Our mouse model did not show that *MYCN* overexpression alone was sufficient for retinoblastoma but revealed extremely potent cooperation with *Rb* loss in driving retinoblastoma. Previous mouse retinoblastoma models required deletion of multiple *Rb* family members (22, 23, 25, 40) or inactivation of *Rb* and the CDK inhibitor *Cdkn1b* (28), events that do not occur in human retinoblastomas. To our knowledge, this is the first mouse retinoblastoma model to recapitulate precise genetic alterations, *Rb* deletion, and the *MYCN* amplifications found in human retinoblastomas.

The key activities of MYCN that drive cancer are unclear, given the pleiotropic functions of MYCN. In the developing retina, we found that MYCN overexpression conferred the ability to bypass a proliferative block that otherwise limited the extent of inappropriate proliferation of *Rb*-deficient cells. Recently, it was shown that, upon *Rb* deletion, MYC can superactivate E2F transcriptional programs, in particular, G_1/S phase–related genes (41). This role for MYC in superactivating E2F targets and driving proliferation in *Rb*-deleted cells may be highly relevant to the retinoblastoma that occurs with *Rb* deletion and *MYCN* amplification, as E2F target gene sets were upregulated in the *Rb/TET-MYCN* retinae com-

pared with what was observed in *Rb*-mutant retinae. The ability of *MYCN* overexpression to obviate any need to inactivate *Rbl1* or *Rbl2* or *Cdkn1b* in driving retinoblastoma is also consistent with key *MYCN* oncogenic functions occurring via proliferation control.

The inducible nature of the current mouse model allowed us to test the requirement of *MYCN* overexpression for retinoblastoma tumor maintenance. Despite the fact that *MYCN* was required for initial tumor emergence in the context of *Rb* deficiency, these tumors evolved to not require *MYCN*. This suggests that therapeutic approaches to reduce MYCN RNA or protein in MYCN-driven retinoblastoma will also likely result in the reemergence of tumors independently of MYCN. In some cases, activation of a *MYCN* target gene, the *Mir-17-92* cluster, occurred. We previously found that *Mir-17-92* functions as a potent oncogene, accelerating retinoblastoma in the *Rb/p107* model (42). *Mir-17-92* is a direct target of *MYCN* (7, 36–38) and probably explains the absence of amplifications in the *Rb/TET-MYCN* DOX-ON condition. Interestingly, a developmental syndrome in humans, Feingold syndrome, is caused by hemizygous *MYCN* loss (43), while a very similar variant syndrome, Feingold syndrome 2, is caused by hemizygous *Mir-17-92* inactivation (44, 45). Given the similar genetic syndromes caused by *MYCN* and *Mir-17-92* hemizygous loss, it is intriguing that *Mir-17-92* amplifications only occurred in the DOX-OFF tumors. In lymphoma models, *Mir-17-92* could partially replace oncogenic functions of the *MYCN* relative *MYC* (46). It is unlikely that *Mir-17-92* completely replaces oncogenic activity of *MYCN* in retinoblastoma, as we could not rescue the impaired proliferation caused by MYCN suppression with *Mir-17-92* overexpression (Supplemental Figure 9, B and C). Also, in contrast to our observations with MYCN overexpression, we previously found that overexpression of *Mir-17-92* did not cooperate with *Rb* loss alone to lead to retinoblastoma, though *Mir-17-92* accelerated retinoblastoma initiated by both *Rb* and *p107* loss (42). In most cases, our CNV analyses of tumors that reemerged in a *MYCN*-independent fashion did not reveal clear amplifications or deletions that could explain the development of *MYCN* independence. In many cases, epigenetic changes in the absence of genetic alterations may contribute to *MYCN* independence. Identification of the mechanisms that retinoblastoma cells in this model undergo to evolve *MYCN* independence is now critical.

In this study, we developed a mouse model that we believe will be invaluable for retinoblastoma preclinical studies, as this is the first mouse retinoblastoma model to our knowledge to be initiated by manipulating only genes that are also mutated in human retinoblastoma. This model revealed that *MYCN*-driven retinoblastoma can evolve to become *MYCN* independent and, we believe, represents an ideal tool for understanding the evolution of *MYCN* independence in *MYCN*-driven cancers.

Methods

Mice. We crossed $Rb^{fl/fl}$ *Pax6* α enhancer *Cre* $Rosa26^{Lox\text{-}STOP\text{-}LOX\text{-}rtTA/+}$ mice (or $Rb^{fl/fl}$, $p107^{-/-}$, *Pax6* α enhancer *Cre*, $Rosa26^{Lox\text{-}STOP\text{-}LOX\text{-}rtTA/+}$ mice) with *TRE-MYCN/LUC* mice (29) to produce mice with inducible *MYCN* transgene expression in distal retina. The $Rb^{fl/fl}$ and $p107^{-/-}$ strains were provided by Tyler Jacks (MIT, Cambridge, Massachusetts, USA); *TRE-MYCN/LUC* mice were provided by William Weiss (UCSF, San Francisco, California, USA); and *Pax6* α enhancer *Cre* mice were provided by Peter Gruss (Max Planck Institute, Gottingen, Germany). DOX was administered in mouse chow at a dose of 625 mg/kg (Harlan Laboratories) without other food sources. For studies of transgene activation, mice were fed DOX chow either during development (DOX food during breeding) or from P21. Mice were monitored for the first visible sign of retinoblastoma, usually involving tumor seeding in the anterior chamber of the eye. We continued to monitor the mice for advanced tumor burden that filled the eye or led to ulceration, at which point the mice were euthanized and tumors collected.

Cell line generation. Retinoblastoma tumor tissue from mouse models was collected using a sterile needle and syringe to extract tumor cells from retinoblastoma-bearing eyes shortly following euthanasia. Tumor tissue was dissociated using a pipette, placed into standard retinoblastoma cell culture, and efficient generation of cell lines from retinoblastoma-bearing mice was observed.

Histology and IHC. Eyes were fixed in Bouin's solution or formalin for 24 hours before paraffin embedment. Paraffin blocks were sectioned at a thickness of 4 μm and stained with H&E. Analysis of general tumor cell morphology was performed by a board-certified pathologist with expertise in ophthalmic pathology (CGE). Immunohistochemical analysis was performed using the following antibodies: p-H3 (1:300; EMD Millipore; catalog 06-570); BrdU (1:300; BD; catalog 347580); and cleaved caspase 3 (1:100; Cell Signaling Technology; catalog 9661). For p-H3 and cleaved caspase 3 staining, paraffin sections were processed from xylene through a graded ethanol series to TBS Tween-20 (TBST). Unmasking was performed using microwave heating in sodium citrate buffer (0.01 M at pH6.0). Endogenous peroxidases were blocked with 3.5% H_2O_2, and immunohistochemical analysis was performed with overnight incubation in primary antibody. Biotin-conjugated secondary antibodies (Vector Laboratories) were used at a dilution of 1:200, and detection was done via a biotin-peroxidase complex (Vectastain ABC; Vector Laboratories) with DAB substrate (Vector Laboratories). For BrdU staining, pepsin digestion was performed by incubation in 0.2 μg/μl pepsin in 10 mM HCl at 37°C. After digestion, slides were denatured and neutralized. Immunohistochemical analysis was performed with an overnight incubation in the primary antibodies. For BrdU analysis, an i.p. injection of pups or adult mice was done with BrdU, and eyes were collected and fixed 1 hour later. TUNEL assays were performed using the In Situ Cell Death Detection Kit, POD (Roche) according to the manufacturer's instructions.

Western blotting. Lysates were prepared in ice-cold RIPA buffer containing protease inhibitor cocktail (Roche) and 1 mM DTT. Western blot assays were conducted with antibodies against MYCN (Santa Cruz Biotechnology Inc.; catalog sc-791); p130 (BD; catalog 610262); p107 (Sigma-Aldrich; catalog P4360); actin (Sigma-Aldrich; catalog A3854); tubulin (Santa Cruz Biotechnology Inc.; catalog sc398103); GAPDH (Santa Cruz Biotechnology Inc.; catalog sc-32233); p21 (Santa Cruz Biotechnology Inc.; catalog sc-397); and p53 (Santa Cruz Biotechnology Inc.; catalog sc-6243). Histone extractions were performed as described previously (47). We used antibodies against histone H3K9Ac (Cell Signaling Technology; catalog 9649P); H3K27Ac (Abcam; catalog ab4729); H3K27me3 (EMD Millipore; catalog 07-449); H4K20me3 (Abcam; catalog ab9053); H2AK5Ac (Cell Signaling Technology; catalog 2576P); H2A (Cell Signaling Technology; catalog 2578P); and H3 (Cell Signaling Technology; catalog 3638).

Quantitative real-time PCR. Total RNA from tumors or cell pellets was isolated with TRIzol (Invitrogen, Thermo Fisher Scientific) and used to synthesize cDNA with iScript Reverse Transcription Supermix (Bio-Rad). Quantitative real-time PCR was performed with ALL-in-ONE qPCR Mix (Genecopoeia) with primers designed to detect human *MYCN* and mouse *Myc*, *Mycn*, *p21*, *p16*, *Igfbp1*, *Igfbp7*, *Il1b*, *Ccr1*, *Il6*, *PAI-1*, and *Gadph* (as an endogenous control). The primer sequences are provided in Supplemental Table 3. Quantitative expression data were acquired and analyzed with a 7900 Real-Time PCR System (Applied Biosystems). The relative copy numbers for *Mycn* and *Mir-17-92* were determined by quantitative real-time PCR using All-in-One qPCR Mix and primers designed to detect murine genomic regions of these genes and *Ant1* (as an endogenous control). Normal tail DNA was used to normalize the data. All samples were analyzed in triplicate.

miR-17~92 overexpression. Retroviral MSCV vectors (empty or overexpressing *Mir-17-92*) were a gift of Andrea Ventura (Memorial Sloan Kettering Institute, New York, New York, USA). MSCV plasmid and plasmids encoding the packaging gene and envelope gene were transfected into 293 cells using Lipofectamine 2000 (Thermo Fisher Scientific). Virus was harvested 3 days after transfection and used for infection of mouse retinoblastoma cell lines. Puromycin (1 μg/ml) was added to cell culture medium for 1 week to select for infected cells. Cells were then expanded for the experiments.

TaqMan small RNA assays. Total RNA from tumors and cell pellets was isolated using TRIzol (Invitrogen, Thermo Fisher Scientific) following the manufacturer's instructions. A TaqMan MicroRNA Reverse Transcription Kit (Applied Biosystems) was used to produce cDNA for TaqMan MicroRNA Assays following the manufacturer's instructions. TaqMan MicroRNA assays to detect miR17 and U6 small nuclear RNA (snRNA) control were obtained from Life Technologies (Thermo Fisher Scientific). Quantitative real-time PCR was performed using TaqMan Universal Master Mix II (Applied Biosystems) on a 7900 Real-Time PCR System (Applied Biosystems).

SA-β-gal activity. Fresh-frozen tissue sections or cells were washed with PBS and fixed in 2% formaldehyde and 0.2% glutaraldehyde. Cells were covered with staining solution (40 mM citric acid/Na phosphate buffer, 5 mM K4[Fe(CN)6] 3H2O, 5 mM K3[Fe(CN)6], 150 mM sodium chloride, 2 mM magnesium chloride, and 1 mg/ml X-gal in distilled water) at 37°C overnight for a total of 16 hours. After incubation, tissue and cells were washed with PBS and methanol and air dried prior to imaging. Tissue from aging WT kidneys was used as a positive control.

Next-generation sequencing analysis. For whole-genome analysis of CNV analysis, we performed low-coverage whole-genome sequencing using DNA from retinoblastomas or matched tails. The NEBNext DNA Library Prep Master Mix Set for Illumina (New England BioLabs; catalog E6040L) was used to generate DNA libraries from 1,000 ng genomic DNA. Single-read data (50 bp) were generated using an Illumina HiSeq 2500. Reads were aligned to the mm9 build of the murine genome using the Burrows Wheeler Aligner (48), and we used CNVseq (49) to examine copy numbers. For RNA-seq analyses, the Ultra RNA Library Prep Kit for Illumina (New England BioLabs; catalog E753L) was used to generate libraries from 500 ng total RNA derived from retinae microdissected at P12. All library preparation was conducted according to the manufacturer's instructions. Single-end sequencing (50 bp) was performed using an Illumina HiSeq 2500, reads were aligned to the mm9 genome using TopHat version 2.08b (50), and Cuffdiff was used to generate the fragment per kilobase per million (FPKM) expression values used for GSEA (http://www.broadinstitute.org/gsea/) (51). Counts were generated from TopHat alignments using the Python package HTSeq v0.5.4p3 (52), using the "intersection-strict" overlap mode. Genes with low counts across conditions were discarded prior to identification of differentially expressed genes using the Bioconductor package edgeR, version 3.4.0 (32). An FDR method was used to correct for multiple testing (53), where differential expression was defined as $|\log_2 (\text{ratio})| \geq 0.585$ (±1.5-fold), with the FDR set at 5%. Overrepresented GO terms for genes that were either significantly up or downregulated were identified with the Bioconductor package goseq, version 1.24.0 (54), using an FDR method to correct for multiple testing. Next-generation sequencing data for this study were deposited in the NCBI's Gene Expression Omnibus (GEO) database (GEO GSE90961).

Statistics. Error bars on all graphs reflect the SD. Comparisons of 2 means were performed using a 2-tailed Student's *t* test. Differences were considered significant at a *P* value of less than 0.05. Kaplan-Meier curves were generated using GraphPad Prism 7 (GraphPad Software), with a log-rank test to determine *P* values for significance.

Study approval. All mouse experiments were conducted in accordance with protocols approved by the IACUC of the Fred Hutchinson Cancer Research Center.

Author contributions

NW and DM designed research studies, analyzed data, and wrote the manuscript. NW, DJ, and BB conducted experiments and analyzed data. RB analyzed data. CGE analyzed the histology of mouse retinoblastomas.

Acknowledgments

We thank members of the Fred Hutchinson Bioinformatics Core, including Jerry Davison, for help with data analysis. This work was supported by National Cancer Institute (NCI) grant R01CA148867 and American Cancer Society Research Scholar Award 120127-RSG-11-270-01-RMC (to DM). We are also grateful to the Elmer and Sylvia Sramek Foundation for study support.

Address correspondence to: David MacPherson, Fred Hutchinson Cancer Research Center, 1100 Fairview Ave N, Seattle, Washington 98109, USA. Phone: 206.667.6464; E-mail: dmacpher@fhcrc.org.

1. Lee WH, Murphree AL, Benedict WF. Expression and amplification of the N-myc gene in primary retinoblastoma. *Nature*. 1984;309(5967):458–460.
2. McEvoy J, et al. RB1 gene inactivation by chromothripsis in human retinoblastoma. *Oncotarget*. 2014;5(2):438–450.
3. Rushlow DE, et al. Characterisation of retinoblastomas without RB1 mutations: genomic, gene expression, and clinical studies. *Lancet Oncol*. 2013;14(4):327–334.
4. Weiss WA, Aldape K, Mohapatra G, Feuerstein BG, Bishop JM. Targeted expression of MYCN causes neuroblastoma in transgenic mice. *EMBO J*. 1997;16(11):2985–2995.
5. Wong AJ, Ruppert JM, Eggleston J, Hamilton SR, Baylin SB, Vogelstein B. Gene amplification of c-myc and N-myc in small cell carcinoma of the lung. *Science*. 1986;233(4762):461–464.
6. O'Donnell KA, Wentzel EA, Zeller KI, Dang CV, Mendell JT. c-Myc-regulated microRNAs modulate E2F1 expression. *Nature*.

2005;435(7043):839–843.
7. Northcott PA, et al. The miR-17/92 polycistron is up-regulated in sonic hedgehog-driven medulloblastomas and induced by N-myc in sonic hedgehog-treated cerebellar neural precursors. *Cancer Res*. 2009;69(8):3249–3255.
8. Schulte JH, et al. MYCN regulates oncogenic MicroRNAs in neuroblastoma. *Int J Cancer*. 2008;122(3):699–704.
9. van Riggelen J, Yetil A, Felsher DW. MYC as a regulator of ribosome biogenesis and protein synthesis. *Nat Rev Cancer*. 2010;10(4):301–309.
10. Lin CY, et al. Transcriptional amplification in tumor cells with elevated c-Myc. *Cell*. 2012;151(1):56–67.
11. Nie Z, et al. c-Myc is a universal amplifier of expressed genes in lymphocytes and embryonic stem cells. *Cell*. 2012;151(1):68–79.
12. Rahl PB, et al. c-Myc regulates transcriptional pause release. *Cell*. 2010;141(3):432–445.
13. Knoepfler PS, Zhang XY, Cheng PF, Gafken PR, McMahon SB, Eisenman RN. Myc influences global chromatin structure. *EMBO J*. 2006;25(12):2723–2734.
14. Otto T, et al. Stabilization of N-Myc is a critical function of Aurora A in human neuroblastoma. *Cancer Cell*. 2009;15(1):67–78.
15. Brockmann M, et al. Small molecule inhibitors of aurora-a induce proteasomal degradation of N-myc in childhood neuroblastoma. *Cancer Cell*. 2013;24(1):75–89.
16. Gustafson WC, et al. Drugging MYCN through an allosteric transition in Aurora kinase A. *Cancer Cell*. 2014;26(3):414–427.
17. Puissant A, et al. Targeting MYCN in neuroblastoma by BET bromodomain inhibition. *Cancer Discov*. 2013;3(3):308–323.
18. Chipumuro E, et al. CDK7 inhibition suppresses super-enhancer-linked oncogenic transcription in MYCN-driven cancer. *Cell*. 2014;159(5):1126–1139.
19. Clarke AR, et al. Requirement for a functional Rb-1 gene in murine development. *Nature*. 1992;359(6393):328–330.
20. Jacks T, Fazeli A, Schmitt EM, Bronson RT, Goodell MA, Weinberg RA. Effects of an Rb mutation in the mouse. *Nature*. 1992;359(6393):295–300.
21. Lee EY, et al. Mice deficient for Rb are nonviable and show defects in neurogenesis and haematopoiesis. *Nature*. 1992;359(6393):288–294.
22. Chen D, Livne-bar I, Vanderluit JL, Slack RS, Agochiya M, Bremner R. Cell-specific effects of RB or RB/p107 loss on retinal development implicate an intrinsically death-resistant cell-of-origin in retinoblastoma. *Cancer Cell*. 2004;5(6):539–551.
23. MacPherson D, Sage J, Kim T, Ho D, McLaughlin ME, Jacks T. Cell type-specific effects of Rb deletion in the murine retina. *Genes Dev*. 2004;18(14):1681–1694.
24. MacPherson D, Conkrite K, Tam M, Mukai S, Mu D, Jacks T. Murine bilateral retinoblastoma exhibiting rapid-onset, metastatic progression and N-myc gene amplification. *EMBO J*. 2007;26(3):784–794.
25. Zhang J, Schweers B, Dyer MA. The first knockout mouse model of retinoblastoma. *Cell Cycle*. 2004;3(7):952–959.
26. Robanus-Maandag E, et al. p107 is a suppressor of retinoblastoma development in pRb-deficient mice. *Genes Dev*. 1998;12(11):1599–1609.
27. Dannenberg JH, Schuijff L, Dekker M, van der Valk M, te Riele H. Tissue-specific tumor suppressor activity of retinoblastoma gene homologs p107 and p130. *Genes Dev*. 2004;18(23):2952–2962.
28. Sangwan M, et al. Established and new mouse models reveal E2f1 and Cdk2 dependency of retinoblastoma, and expose effective strategies to block tumor initiation. *Oncogene*. 2012;31(48):5019–5028.
29. Swartling FJ, et al. Pleiotropic role for MYCN in medulloblastoma. *Genes Dev*. 2010;24(10):1059–1072.
30. Marquardt T, Ashery-Padan R, Andrejewski N, Scardigli R, Guillemot F, Gruss P. Pax6 is required for the multipotent state of retinal progenitor cells. *Cell*. 2001;105(1):43–55.
31. Mendoza PR, et al. Histopathologic grading of anaplasia in retinoblastoma. *Am J Ophthalmol*. 2015;159(4):764–776.
32. Robinson MD, McCarthy DJ, Smyth GK. edgeR: a Bioconductor package for differential expression analysis of digital gene expression data. *Bioinformatics*. 2010;26(1):139–140.
33. Boon K, et al. N-myc enhances the expression of a large set of genes functioning in ribosome biogenesis and protein synthesis. *EMBO J*. 2001;20(6):1383–1393.
34. Zhang J, et al. Rb regulates proliferation and rod photoreceptor development in the mouse retina. *Nat Genet*. 2004;36(4):351–360.
35. Podsypanina K, Politi K, Beverly LJ, Varmus HE. Oncogene cooperation in tumor maintenance and tumor recurrence in mouse mammary tumors induced by Myc and mutant Kras. *Proc Natl Acad Sci USA*. 2008;105(13):5242–5247.
36. Mestdagh P, et al. MYCN/c-MYC-induced microRNAs repress coding gene networks associated with poor outcome in MYCN/c-MYC-activated tumors. *Oncogene*. 2010;29(9):1394–1404.
37. Fontana L, et al. Antagomir-17-5p abolishes the growth of therapy-resistant neuroblastoma through p21 and BIM. *PLoS One*. 2008;3(5):e2236.
38. Lovén J, et al. MYCN-regulated microRNAs repress estrogen receptor-alpha (ESR1) expression and neuronal differentiation in human neuroblastoma. *Proc Natl Acad Sci USA*. 2010;107(4):1553–1558.
39. Mu P, et al. Genetic dissection of the miR-17~92 cluster of microRNAs in Myc-induced B-cell lymphomas. *Genes Dev*. 2009;23(24):2806–2811.
40. Conkrite K, Sundby M, Mu D, Mukai S, MacPherson D. Cooperation between Rb and Arf in suppressing mouse retinoblastoma. *J Clin Invest*. 2012;122(5):1726–1733.
41. Liu H, et al. Redeployment of Myc and E2f1-3 drives Rb-deficient cell cycles. *Nat Cell Biol*. 2015;17(8):1036–1048.
42. Conkrite K, et al. miR-17~92 cooperates with RB pathway mutations to promote retinoblastoma. *Genes Dev*. 2011;25(16):1734–1745.
43. van Bokhoven H, et al. MYCN haploinsufficiency is associated with reduced brain size and intestinal atresias in Feingold syndrome. *Nat Genet*. 2005;37(5):465–467.
44. Grote LE, Repnikova EA, Amudhavalli SM. Expanding the phenotype of feingold syndrome-2. *Am J Med Genet A*. 2015;167A(12):3219–3225.
45. de Pontual L, et al. Germline deletion of the miR-17~92 cluster causes skeletal and growth defects in humans. *Nat Genet*. 2011;43(10):1026–1030.
46. Li Y, Choi PS, Casey SC, Dill DL, Felsher DW. MYC through miR-17-92 suppresses specific target genes to maintain survival, autonomous proliferation, and a neoplastic state. *Cancer Cell*. 2014;26(2):262–272.
47. Shechter D, Dormann HL, Allis CD, Hake SB. Extraction, purification and analysis of histones. *Nat Protoc*. 2007;2(6):1445–1457.
48. Li H, Durbin R. Fast and accurate long-read alignment with Burrows-Wheeler transform. *Bioinformatics*. 2010;26(5):589–595.
49. Xie C, Tammi MT. CNV-seq, a new method to detect copy number variation using high-throughput sequencing. *BMC Bioinformatics*. 2009;10:80.
50. Trapnell C, Pachter L, Salzberg SL. TopHat: discovering splice junctions with RNA-Seq. *Bioinformatics*. 2009;25(9):1105–1111.
51. Subramanian A, et al. Gene set enrichment analysis: a knowledge-based approach for interpreting genome-wide expression profiles. *Proc Natl Acad Sci USA*. 2005;102(43):15545–15550.
52. Anders S, Pyl PT, Huber W. HTSeq--a Python framework to work with high-throughput sequencing data. *Bioinformatics*. 2015;31(2):166–169.
53. Reiner A, Yekutieli D, Benjamini Y. Identifying differentially expressed genes using false discovery rate controlling procedures. *Bioinformatics*. 2003;19(3):368–375.
54. Young MD, Wakefield MJ, Smyth GK, Oshlack A. Gene ontology analysis for RNA-seq: accounting for selection bias. *Genome Biol*. 2010;11(2):R14.